Available online at www.sciencedirect.com
SCIENCE DIRECT®
Journal of Solid State Chemistry 178 (2005) 1753–1764
JOURNAL OF SOLID STATE CHEMISTRY
www.elsevier.com/locate/jssc

Crystal structures of the ionic conductors $Bi_{46}M_8O_{89}$ (M = P, V) related to the fluorite-type structure

J. Darriet[a,*], J.C. Launay[a], F.J. Zúniga[b]

[a]*Institut de Chimie de la Matière Condensée de Bordeaux (ICMCB), UPR9048 CNRS, Université de Bordeaux 1, 87 Avenue du Docteur Albert Schweitzer, Pessac Cedex FR-33608, France*
[b]*Facultad de Ciencias, Departamento de Fisica de la Materia Condensada, Universidad del Pais Vasco, Apdo 644, Bilbao 48080, Spain*

Received 10 February 2005; received in revised form 8 March 2005; accepted 8 March 2005
Available online 15 April 2005

Abstract

The crystal structures of the two oxides $Bi_{46}M_8O_{89}$ (M = P, V) have been solved from single crystals X-ray data at room temperature. $Bi_{46}P_8O_{89}$ crystallizes in the monoclinic symmetry (space group $C2/m$) with the cell parameters $a = 19.6073(4)$ Å, $b = 11.4181(4)$ Å, $c = 21.1119(4)$ Å and $\beta = 112.14(3)^\circ$. The symmetry of $Bi_{46}V_8O_{89}$ is also monoclinic but the space group is $P2_1/c$ with the unit-cell parameters: $a = 20.0100(4)$ Å, $b = 11.6445(4)$ Å, $c = 20.4136(4)$ Å and $\beta = 107.27(3)^\circ$. Both structures derive from an oxygen deficient fluorite-type structure where the Bi and M cations (M = P, V) are ordered in the framework. The structures are characterised by isolated MO_4 tetrahedra (M = P, V) which contradicts the previous results. The difference between the two structures is only due to a different order of the M atoms (M = P, V) in the fluorite-type superstructure. It will be shown that some oxygen sites are partially occupied in both structures which can explain the ion conduction properties of these phases. A structural building principle will be proposed that can explain the large domain of solid solution related to the fluorite-type observed in both systems.

Keywords: Phosphorous; Vanadium; Bismuth; Oxides; Crystal structures; Fluorite-type superstructure

1. Introduction

It is well known that bismuth sesquioxide is a good ionic conductor in its high temperature cubic fluorite form [1–3] resulting from the structural disorder in the O sublattice. This δ-Bi_2O_3 variety is stable only between 937 K and the melting point of Bi_2O_3 at 1097 K. However this variety can be stabilized at room temperature by doping with many other metal oxides. Among the mixed bismuth oxides, the Bi_2O_3–V_2O_5 system has widely been studied by electron diffraction [4,5] and X-ray diffraction [6–9]. These studies show that there are numerous phases for low concentrations of vanadium, especially for compositions from $9Bi_2O_3$–$1V_2O_5$ to $7Bi_2O_3$–$2V_2O_5$. All the proposed structures in this range of compositions correspond to superstructures based on a fluorite pseudo-*fcc* subcell. However, a careful examination of the literature [4–9] show inconsistencies in the number and composition of the phases. A chronological view of the contradictory results is gathered in [8]. Different structural models have been proposed but exact details of the structures have not been given yet. As an example, it has been proposed that the compounds corresponding to composition ranging between $6Bi_2O_3$–$1V_2O_5$ and $7Bi_2O_3$–$2V_2O_5$ have structural types designated as type II with six different structures [4,5]. For all the structures, it has been assumed that vanadium cations exist in the form of V_4O_{10} clusters inside the defect fluorite δ-Bi_2O_3 host lattice. These V_4O_{10} clusters result from tetrahedra sharing corners and are ordered on one of the (111) planes of the fluorite lattice [5]. These conclusions result

*Corresponding author. Fax: +33 5 40 00 27 61.
E-mail address: darriet@icmcb-bordeaux.cnrs.fr (J. Darriet).

0022-4596/$ - see front matter © 2005 Elsevier Inc. All rights reserved.
doi:10.1016/j.jssc.2005.03.013

from high resolution electron microscopy investigations but are in contradiction with preliminary approaches of the structures on single crystals [6,7]. To resume, the structure of these phases is not well defined and therefore we decided to tackle the problem. This paper is devoted to the crystal structure of $Bi_{46}V_8O_{89}$ which belongs to this family and for which it is clear, from the literature, that this composition corresponds to a single phase [7–9]. Also, in the present work, the crystal structure of the phosphorus homologous $Bi_{46}P_8O_{89}$ has been solved on single crystal. It will be shown that both structures are not perfectly isostructural, but correspond to the same member of a new family of structures related to the fluorite-type structure.

2. Experimental

A polycrystalline sample of $Bi_{46}V_8O_{89}$ was prepared using standard ceramic techniques. The starting oxides α-Bi_2O_3 and V_2O_5 of purity 6N were mixed in molar ratio 23:4 and ground in an agate mortar. The mixture was heated at 600 °C for 12 h in a gold crucible and under oxygen atmosphere. Then, after regrinding, the temperature was increased slowly to 850 °C for 3 days. It is known that $Bi_{46}V_8O_{89}$ melts congruently at about 950 °C without polymorphic transformation [8]. Single crystals of $Bi_{46}V_8O_{89}$ have been prepared in solid phase by heating the pulverulent sample at 940 °C during a period of 10 days and cooled slowly at a rate of 4 °C h^{-1} down to 300 °C, afterwards turning off the power of the furnace. Pale yellow crystals with the morphology of thin plates stacked perpendicular to the *c*-axis can be observed under microscope. Preliminary studies undertaken on Kappa CCD (Bruker-Nonius) four circles diffractometer with Mo$K\alpha$ X-ray radiation shows that the majority of the crystals are twinned by rotation around the *c**-axis as it had been observed previously [7]. After several tests, a very thin plate (0.005 mm of thickness) has been checked of good quality and selected for data collection.

A pulverulent sample (~6 g mass) of $Bi_{23}P_4O_{44.5}$ was synthesized from the starting materials V_2O_5 and $(NH_4)H_2PO_4$. The stoichiometric proportions were accurately weighed and thoroughly hand mixed in an agate mortar. The mixture was heated in a gold crucible at 400 °C for 24 h under oxygen atmosphere and then the temperature was gradually increased up to 850 °C for 2 days. After regrinding, the product was reheated at 850 °C for 3 days. Single crystals of $Bi_{23}P_4O_{44.5}$ were grown by melting the polycrystalline sample at 950 °C during 4 h and cooled slowly at a rate of 4 °C h^{-1} down to room temperature. It appears that the selection of a good single crystal (colourless) for data collection is less hard than for the vanadium crystals.

Data collections were performed on an Kappa CCD (Bruker-Nonius) diffractometer. The frame images were integrated using Eval-14 software [10]. Measured intensities were corrected for Lorentz and polarisation effects. Absorption corrections were applied by using the Gaussian method. The shape of the crystals was determined via the video camera of the diffractometer. The structures were solved using the JANA2000 package [11].

3. Results and discussion

3.1. Structure of $Bi_{46}V_8O_{89}$

A standard peak search shows that the main peaks can be indexed with a *C*-centred monoclinic unit-cell with lattice parameters of $a = 20.0100(4)$ Å, $b = 11.6445(4)$ Å, $c = 20.4136(4)$ Å and $\beta = 107.27(3)°$. Crystal data and experimental conditions of the data collection are gathered in Table 1. A reciprocal space reconstruction from the data shows that weak reflections cannot be indexed in the *C*-centred Bravais lattice as shown for the (*h*0*l*) plane (Fig. 1). The observed extinction rules suggest the space group $P2_1/c$. If one neglects the weak reflections, the possible space groups are: $C2/c$ (centrosymmetric) or Cc (non-centrosymmetric). The strongest reflections correspond to a fluorite subcell. The relationship between the monoclinic cell and the cubic fluorite subcell is:

$$\mathbf{a} = 3/2\mathbf{a}_c + 3/2\mathbf{b}_c + 3\mathbf{c}_c,$$
$$\mathbf{b} = -3/2\mathbf{a}_c + 3/2\mathbf{b}_c,$$
$$\mathbf{c} = -5/2\mathbf{a}_c - 5/2\mathbf{b}_c + \mathbf{c}_c,$$

where $\mathbf{a}_c$, $\mathbf{b}_c$ and $\mathbf{c}_c$ are the unit-cell vectors of the prototypic cubic fluorite ($\mathbf{a}_c \approx 5.5$ Å). Therefore, the unit-cell lengths can be approximated as: $a \approx c \approx 3\sqrt{6}/2a_c$, $b = 3\sqrt{2}/2a_c$ and $\sin\beta = 4(3\sqrt{2})$ ($\beta \approx 109.45°$) what leads to a volume of the monoclinic unit-cell 27 times larger than the elementary volume of the fluorite. One can also notice that all the strong reflections can be indexed using a triclinic unit-cell as it has been proposed in Ref. [5] for the type IIc.

In a first step, the structure of $Bi_{46}V_8O_{49}$ ($Z = 2$) has been determined using only the strong reflections which correspond to a C-based centred symmetry. The positions of the heavy atoms were deduced from a Patterson map. All the 108 heavy atoms of the unit-cell correspond to 14 independent positions for Bi and 2 independent sites for V. The refinement with the $C2/c$ centrosymmetric space group and isotropic displacement parameters (ADP) leads to a *R*-factor value of 0.123 for 4034 independent reflections. All the ADP parameters have an average value close to $U_{iso} \approx 0.015$ Å^2 except for three Bi positions (Bi6, Bi8 and

Table 1
Crystallographic data for $Bi_{46}V_8O_{89}$

Physical, crystallographic and analytical data	
Formula	$Bi_{46}V_8O_{89}$
Crystal colour	Pale yellow
MW ($g\,mol^{-1}$)	11444.6
Crystal system	Monoclinic
Space group	$P2_1/c$
Parameters	$a = 20.0100(3)$ Å, $b = 11.6445(2)$ Å, $c = 20.4136(4)$ Å, $\beta = 107.27(3)^\circ$
V (Å^3)	4542.1(6)
Z	2
Density calc. ($g\,cm^{-3}$)	8.365
Crystal shape	Plate
Crystal size (mm)	$0.035 \times 0.018 \times 0.0025$
Data collection	
Temperature	RT
Diffractometer	Bruker-Nonius KappaCCD
Radiation	Mo$K\alpha$ ($\lambda = 0.71069$ Å)
Scan mode	CCD scan
hkl range	$-35<h<36$ $-21<k<21$ $-36<l<36$
θ_{max}	40°
Data reduction	
Linear absorption coeff.	$89.62\,mm^{-1}$
Absorption correction	Gaussian
T_{min}/T_{max}	0.042/0.471
No of reflections	28,062
No of independent reflections	5669
Criterion for obs. Reflections	$I > 3\sigma(I)$
Refinement results	
Refinement	F^2
$F(000)$	9428
R factors	$R(F) = 0.0582$, $wR(F^2) = 0.0982$
No of refined parameters	426
g.o.f.	1.16
Weighting scheme	$w = 1/(\sigma^2(I) + 0.0009I^2)$
Diff. Fourier residues (e^-/Å^3)	[−4.54, +4.53]

Bi9) with ADP values three times larger. Fourier maps around these positions revealed that the initially Bi6 position should be split in two positions (Bi6 and Bi6*a*). In a similar way, the two special positions (Bi8 and Bi10) initially in 4*e* Wyckoff notation are split in 8*f* general position (Table 2). The *R*-value decreases to 0.111 with an occupancy factor of the Bi6 and Bi6*a* positions of ≈25% and 75%, respectively. Then, the harmonic displacement parameters of all the atoms (Bi + V) have been considered in the refinement and the *R*-value decreases down to 0.0778 for 133 variable parameters. At this stage of the refinement, the oxygen positions were deduced from successive difference Fourier maps. Clearly, 13 oxygen positions were localised which correspond to oxygen only bonded to the bismuth atoms. Difference Fourier maps around the two independent vanadium sites (V1 and V2) show that all the oxygen atoms linked to the V atoms are systematically split in two positions (Ov_{1-8} and Ov_{1a-8a}) (Table 2). The residual *R* factor converged to $R = 0.0522$ for 242 variable parameters. All the oxygen positions have only been refined with isotropic displacement parameters. At this stage of the refinement, the charge balance that corresponds to the formula "$Bi_{46}V_8O_{84}$" is not fulfilled. A final difference Fourier shows three oxygen positions (Ox1, Ox2 and Ox3 in 8*f* position), which are partially occupied with a rate of 75%, 25% and 25%, respectively. Then, the global formula $Bi_{46}V_8O_{49}$ is fulfilled. The residue factors are clearly improved considering these three oxygen positions and decrease down to $R = 0.0484$, $wR(F^2) = 0.084$ (g.o.f. = 1.10) for 255 variables parameters and 4034 independent reflections. Final parameters are gathered in Table 2.

The next stage in the refinement was to consider the weak reflections. As it is shown in Fig. 1(b), the C centered symmetry is not satisfied. Therefore the Bravais lattice is primitive and an examination of the main reciprocal planes leads to the symmetrical $P2_1/c$ space group. The independent atomic positions have been

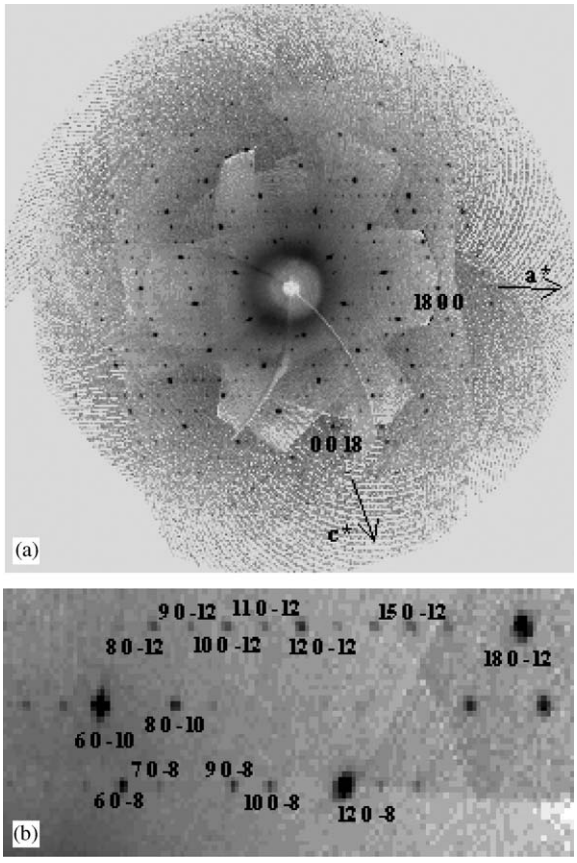

Fig. 1. (a) ($h0l$) plane of $Bi_{46}V_8O_{89}$; (b) zoom showing the weak peaks corresponding to the primitive unit-cell ($P2_1/c$).

deduced from those of the C centred sublattice using the options of the JANA program [11]. One should notice that the translation of $\frac{1}{4}$, $\frac{1}{4}$, 0 of the origin has been made to get the standard representation of the $P2_1/c$ space group of the International Tables. The refinement converged to the residual values $R = 0.0551$, $wR(F^2) = 0.093$ for 5669 independent reflections ($I > 3s(I)$) (Table 1). The fractional atomic coordinates and the ADP are gathered in Table 3. Obviously, the general position (8*f*) of the C centred sub-structure is split in two 4*e* general position for the $P2_1/c$ space group. Therefore the majority of the bismuth and vanadium atomic positions are split except the special position Bi9 and those where a partial occupancy has been introduced in the previous refinement (see Table 2). The refinement revealed that the Bi6/Bi6*a* positions where a disordering had been introduced (Table 2), are perfectly ordered in the two positions Bi11 and Bi12 (Table 3). The second observation concerns the Bi8 and Bi10 sites (see Table 2) that had been delocalised previously and which are now totally ordered in the two positions Bi15 and Bi17, respectively (Table 3). A similar result is observed for the oxygen bonded to the vanadium atoms (Ov1 to Ov8*a* in Table 2), also ordered in the structure (positions O27 to O42 in the Table 3). The interesting results concern the oxygen sites Ox1, Ox2 and Ox3, previously partially occupied (Table 2). The lowering of the Bravais lattice to the primitive space group $P2_1/c$ should have resulted in six related positions. The refinement revealed that only four of the positions are occupied and moreover one of these is fully occupied (O43) (Table 3). From these structural results, one can presume that the pathway of the ionic conductivity of $Bi_{46}V_8O_{89}$ is assumed through the O44, O45 and O46 sites that are partially occupied (Table 3).

A collect of the data has been carried out at low temperature ($T = 100$ K) in order to observe an eventually lowering of the symmetry related to a structural order of the oxygen atoms. The results will be not detailed here but it appears that the symmetry and the space group remain identical. The unit-cell parameters are: $a = 19.9707(4)$ Å, $b = 11.6028(3)$ Å, $c = 20.3549(4)$ Å) and $\beta = 107.27(2)^\circ$ and the refinement leads to the *R*-value = 0.065 for 5152 independent reflections. The structure is similar to that at room temperature except the obvious systematic decrease of the atomic displacement parameters for all the atoms.

A view of the structure of $Bi_{46}V_8O_{89}$ projected on the (001) plane is given in Fig. 2. The main observation that can be done is that the VO4 tetrahedra are definitely isolated to ones from the others in contrast with the previous assumption where V4O10 clusters have been postulated [4,5]. The V–O distances in the tetrahedra are gathered in Table 4. The vanadium–oxygen distances range between 1.56(4) and 1.81(2) Å and are consistent with pentavalent vanadium. One can notice a rather short V–O distance (V1–O35 = 1.56(4) Å) that is not so unusual for pentavalent vanadium. For example, such short distance is observed in the structure of V_2O_5 (1.576 Å) [12]. Generally, this short distance is associated to a long V–O distance as it is the case for the V1 tetrahedron (Table 4). If one limits the Bi–O distances involved in the surroundings of the bismuth to 2.5 Å, three different types of polyhedra are observed (Fig. 3). The coordination number can vary from CN = 3 to 5 (Fig. 3) and in all the cases the $6s^2$ lone pair of Bi^{III} is stereochemically active. As mentioned previously, the O44, O45 and O46 positions are half occupied (Table 3). These oxygen atoms can be bonded to Bi6, Bi10 or Bi21 (Table 3). For example, a representation of the environment around Bi6 is shown in Fig. 3d. Obviously, all these positions cannot be fully occupied simultaneously but different configurations can be figured out. In the unit-cell, one must have 178 oxygen atoms ($Z = 2$ for $Bi_{46}V_8O_{89}$). 172 oxygen atoms correspond to the O1 to O43 positions (Table 3), therefore one must distribute six supplementary oxygen atoms between the three positions O44, O45 and O46. All these positions correspond to a 4*e* general position (Table 3). If the O46 position is fully occupied which can be possible as

Table 2
Final coordinates, equivalent displacement parameters (Bi, V) and isotropic displacement parameters (O) for $Bi_{46}V_8O_{89}$ for the C centred monoclinic symmetry ($C2/c$ space group)

Atoms	Wyckoff position	Occupancy	X	y	z	$U_{eq}(\text{Å}^2)/U_{iso}(\text{Å}^2)$
V1	8*f*	1	0.0663(2)	0.3901(3)	0.1064(2)	0.020(1)
V2	8*f*	1	0.2366(2)	0.9011(3)	0.0819(2)	0.019(1)
Bi1	8*f*	1	0.05482(4)	0.04918(7)	0.08025(5)	0.0188(3)
Bi2	8*f*	1	0.06301(4)	0.74402(7)	0.08933(5)	0.0183(3)
Bi3	8*f*	1	0.22693(4)	0.22316(7)	0.08881(5)	0.0227(3)
Bi4	8*f*	1	0.22374(4)	0.55296(7)	0.07951(5)	0.0180(3)
Bi5	8*f*	1	0.40467(4)	0.07099(7)	0.08362(5)	0.0230(3)
Bi6	8*f*	0.24(2)	0.3829(5)	0.4100(10)	0.0886(5)	0.0173(6)
Bi6*a*	8*f*	0.76(2)	0.3823(1)	0.3770(5)	0.0942(2)	0.0173
Bi7	8*f*	1	0.39791(4)	0.70975(7)	0.08132(5)	0.0189(3)
Bi8	8*f*	0.5	0.0082(3)	0.0705(1)	0.2610(2)	0.022(1)
Bi9	4*e*	1	0	0.3881(1)	1/4	0.0208(4)
Bi10	8*f*	0.5	0.9935(2)	0.70489(1)	0.2583(3)	0.020(1)
Bi11	8*f*	1	0.17629(4)	0.21361(7)	0.27623(5)	0.0247(3)
Bi12	8*f*	1	0.17320(4)	0.56664(7)	0.25734(5)	0.0176(3)
Bi13	8*f*	1	0.15764(4)	0.90022(7)	0.24313(5)	0.0204(3)
O1	8*f*	1	0.1133(6)	0.0828(10)	0.2245(7)	0.021(3)
O2	8*f*	1	0.0748(6)	0.8951(9)	0.1501(6)	0.018(3)
O3	8*f*	1	0.9675(6)	0.0620(9)	0.1166(6)	0.016(3)
O4	8f	1	0.0248(7)	0.8952(11)	0.0184(7)	0.031(3)
O5	8*f*	1	0.2734(6)	0.3920(10)	0.1065(7)	0.022(3)
O6	8*f*	1	0.4621(6)	0.2301(10)	0.1038(7)	0.023(3)
O7	8*f*	1	0.9172(6)	0.8840(10)	0.2005(7)	0.027(3)
O8	8*f*	1	0.9396(7)	0.2419(11)	0.1901(8)	0.029(3)
O9	8*f*	1	0.2665(6)	0.0784(10)	0.3147(7)	0.024(3)
O10	8*f*	1	0.3962(8)	0.1978(13)	0.2944(9)	0.046(4)
O11	8*f*	1	0.1725(6)	0.1109(11)	0.3791(7)	0.033(3)
O12	8*f*	1	0.0630(8)	0.5561(12)	0.3112(9)	0.045(4)
O13	8*f*	1	0.2564(9)	0.2045(14)	0.2008(9)	0.058(5)
Ov1	8*f*	0.5	0.320(2)	0.889(3)	0.085(2)	0.035(5)
Ov1*a*	8*f*	0.5	0.330(2)	0.882(3)	0.107(2)	0.035
Ov2	8*f*	0.5	0.196(2)	0.958(3)	0.001(2)	0.040(6)
Ov2*a*	8*f*	0.5	0.218(2)	0.007(3)	0.023(2)	0.040
Ov3	8*f*	0.5	0.198(1)	0.774(2)	0.093(2)	0.032(5)
Ov3*a*	8*f*	0.5	0.200(2)	0.776(3)	0.0588(2)	0.032
Ov4	8*f*	0.5	0.217(2)	0.000(2)	0.133(2)	0.037(5)
Ov4*a*	8*f*	0.5	0.224(1)	0.944(2)	0.158(2)	0.037
Ov5	8*f*	0.5	0.137(2)	0.392(3)	0.088(2)	0.051(6)
Ov5*a*	8*f*	0.5	0.122(2)	0.381(3)	0.054(2)	0.051
Ov6	8*f*	0.5	0.012(2)	0.280(3)	0.069(2)	0.055(8)
Ov6*a*	8*f*	0.5	0.994(2)	0.323(3)	0.070(2)	0.055
Ov7	8*f*	0.5	0.021(2)	0.514(3)	0.078(2)	0.063(8)
Ov7*a*	8*f*	0.5	0.041(2)	0.518(3)	0.118(2)	0.063
Ov8	8*f*	0.5	0.073(1)	0.386(3)	0.199(2)	0.039(6)
Ov8*a*	8*f*	0.5	0.112(1)	0.337(2)	0.186(2)	0.039(6)
Ox1	8*f*	0.75	0.3285(9)	0.1979(15)	0.0805(10)	0.026(4)
Ox2	8*f*	0.25	0.3294(3)	0.1430(4)	0.1399(29)	0.026
Ox3	8*f*	0.25	0.3072(26)	0.2203(42)	0.02399(31)	0.026

the O46–$O46_{eq}$ distance is compatible (2.30 Å) (Fig. 3d), the two missing oxygen atoms can only occupy the O45 position ($d_{O46-O45} = 2.54$ Å). Indeed, the O46–O43 distance of 1.38 Å is absolutely unrealistic. The second possible configuration corresponds to the trivial reverse situation when the O45 position is fully occupied. Finally, a third possibility can be considered, that is when the O44 position is occupied. In this case, this position can only be half occupied. Indeed, the O–O distances between O44 and O45 or O46 are too short (≈ 1.38 Å) for a fully occupancy of the O44 site. Consequently, the four missing oxygen atoms are partially distributed between the O46 and O45 sites. One can notice that whatever the different

Table 3
Final coordinates, equivalent displacement parameters (Bi, V) and isotropic displacement parameters (O) for $Bi_{46}V_8O_{89}$ for the primitive monoclinic symmetry ($P2_1/c$ space group)

Atoms	Wyckoff position	Occupancy	x	y	z	$U_{eq}(\AA^2)/U_{iso}(\AA^2)$
V1	4*e*	1	0.3144(4)	0.6407(5)	0.1079(4)	0.019(3)
V2	4*e*	1	0.8181(3)	0.1395(6)	0.1052(4)	0.020(3)
V3	4*e*	1	0.4831(4)	0.1539(5)	0.0810(4)	0.016(3)
V4	4*e*	1	0.9904(3)	0.6487(6)	0.0838(4)	0.019(3)
Bi1	4*e*	1	0.30281(8)	0.29678(13)	0.07637(9)	0.0161(6)
Bi2	4*e*	1	0.80672(8)	0.80173(13)	0.08416(9)	0.0161(6)
Bi3	4*e*	1	0.30985(8)	0.99155(13)	0.08544(9)	0.0146(5)
Bi4	4*e*	1	0.81619(8)	0.49672(13)	0.09338(9)	0.0156(5)
Bi5	4*e*	1	0.47726(8)	0.47264(14)	0.09265(9)	0.0179(6)
Bi6	4*e*	1	0.97663(9)	0.97372(14)	0.08490(9)	0.0230(7)
Bi7	4*e*	1	0.47251(8)	0.80448(14)	0.08279(9)	0.0154(6)
Bi8	4*e*	1	0.97492(8)	0.30139(13)	0.07622(9)	0.0159(6)
Bi9	4*e*	1	0.66034(8)	0.31879(14)	0.08452(9)	0.0163(5)
Bi10	4*e*	1	0.14863(9)	0.82379(14)	0.08282(9)	0.0194(5)
Bi11	4*e*	1	0.63338(8)	0.6298(13)	0.09550(9)	0.0163(5)
Bi12	4*e*	1	0.13166(9)	0.14304(17)	0.09033(9)	0.0318(7)
Bi13	4*e*	1	0.64799(8)	0.95272(13)	0.08088(9)	0.0156(5)
Bi14	4*e*	1	0.14777(8)	0.46687(13)	0.08167(9)	0.0167(6)
Bi15	4*e*	1	0.24275(10)	0.32058(12)	0.24006(10)	0.0272(7)
Bi16	4*e*	1	0.24891(10)	0.63811(10)	0.25476(10)	0.0167(4)
Bi17	4*e*	1	0.25332(10)	0.95473(11)	0.24038(10)	0.0236(5)
Bi18	4*e*	1	0.42200(8)	0.46149(12)	0.28026(9)	0.0189(6)
Bi19	4*e*	1	0.93039(8)	0.96583(12)	0.27241(9)	0.0162(5)
Bi20	4*e*	1	0.42238(8)	0.81341(14)	0.25875(9)	0.0167(6)
Bi21	4*e*	1	0.92409(8)	0.32000(15)	0.25600(9)	0.0158(6)
Bi22	4*e*	1	0.40830(8)	0.15371(15)	0.24005(8)	0.0204(6)
Bi23	4*e*	1	0.90696(8)	0.64714(13)	0.24601(8)	0.0157(6)
O1	4*e*	1	0.363(1)	0.331(2)	0.223(1)	0.019(5)
O2	4*e*	1	0.864(1)	0.834(2)	0.223(1)	0.019(5)
O3	4*e*	1	0.325(1)	0.139(2)	0.148(1)	0.019(5)
O4	4*e*	1	0.824(1)	0.651(2)	0.153(1)	0.012(5)
O5	4*e*	1	0.217(1)	0.313(2)	0.116(1)	0.008(5)
O6	4*e*	1	0.718(1)	0.810(2)	0.117(1)	0.026(6)
O7	4*e*	1	0.269(1)	0.140(2)	0.016(1)	0.028(6)
O8	4*e*	1	0.781(1)	0.650(2)	0.022(1)	0.020(5)
O9	4*e*	1	0.521(1)	0.644(2)	0.103(1)	0.032(7)
O10	4*e*	1	0.025(1)	0.141(2)	0.110(1)	0.011(5)
O11	4*e*	1	0.712(1)	0.482(2)	0.100(1)	0.018(5)
O12	4*e*	1	0.212(1)	0.979(2)	0.107(1)	0.023(6)
O13	4*e*	1	0.171(1)	0.144(2)	0.199(1)	0.010(4)
O14	4*e*	1	0.664(1)	0.623(2)	0.203(1)	0.025(6)
O15	4*e*	1	0.197(1)	0.490(2)	0.191(1)	0.023(6)
O16	4*e*	1	0.682(1)	0.994(2)	0.189(1)	0.019(5)
O17	4*e*	1	0.515(1)	0.323(2)	0.310(1)	0.015(5)
O17	4*e*	1	0.515(1)	0.323(2)	0.310(1)	0.015(5)
O18	4*e*	1	0.018(1)	0.834(2)	0.320(1)	0.024(6)
O19	4*e*	1	0.652(1)	0.435(2)	0.299(1)	0.028(6)
O20	4*e*	1	0.139(1)	0.961(2)	0.290(1)	0.034(7)
O21	4*e*	1	0.424(1)	0.365(2)	0.374(1)	0.012(4)
O22	4*e*	1	0.920(1)	0.854(2)	0.386(1)	0.040(7)
O23	4*e*	1	0.320(1)	0.814(2)	0.310(1)	0.018(5)
O24	4*e*	1	0.804(1)	0.297(2)	0.313(1)	0.033(7)
O25	4*e*	1	0.519(1)	0.463(2)	0.197(2)	0.046(8)
O26	4*e*	1	0.997(1)	0.948(2)	0.204(1)	0.023(6)
O27	4*e*	1	0.568(2)	0.143(2)	0.091(2)	0.055(9)
O28	4*e*	1	0.080(1)	0.630(2)	0.101(1)	0.026(6)
O29	4*e*	1	0.445(1)	0.205(2)	0.999(2)	0.050(8)
O30	4*e*	1	0.965(1)	0.754(2)	0.022(1)	0.041(7)
O31	4*e*	1	0.449(1)	0.027(2)	0.093(1)	0.036(7)
O32	4*e*	1	0.950(1)	0.524(2)	0.061(1)	0.040(7)
O33	4*e*	1	0.468(1)	0.250(2)	0.135(1)	0.022(5)

Table 3 (*continued*)

Atoms	Wyckoff position	Occupancy	x	y	z	$U_{eq}(\AA^2)/U_{iso}(\AA^2)$
O34	4*e*	1	0.973(1)	0.691(2)	0.158(2)	0.053(8)
O35	4*e*	1	0.386(2)	0.639(3)	0.092(2)	0.09(1)
O36	4*e*	1	0.875(1)	0.137(2)	0.058(1)	0.034(6)
O37	4*e*	1	0.260(2)	0.538(3)	0.070(2)	0.08(1)
O38	4*e*	1	0.749(2)	0.057(3)	0.072(2)	0.07(1)
O39	4*e*	1	0.273(2)	0.760(4)	0.081(2)	0.11(1)
O40	4*e*	1	0.788(2)	0.270(2)	0.114(2)	0.057(9)
O41	4*e*	1	0.324(1)	0.636(2)	0.199(1)	0.026(6)
O42	4*e*	1	0.864(2)	0.089(3)	0.187(2)	0.062(9)
O43	4*e*	1	0.578(1)	0.449(2)	0.076(1)	0.019(5)
O44	4*e*	0.5	0.078(2)	0.946(4)	0.094(3)	0.018(6)
O45	4*e*	0.5	0.081(2)	0.890(4)	0.145(2)	0.018
O46	4*e*	0.5	0.057(2)	0.973(3)	0.025	0.018

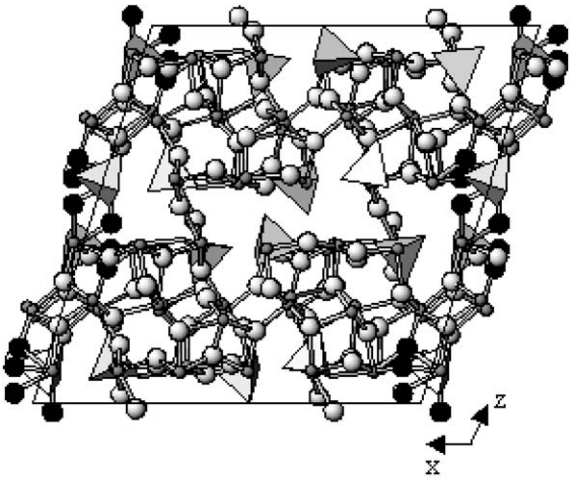

Fig. 2. View of the $Bi_{46}V_8O_{89}$ structure projected on the (010) plane. Tetrahedra correspond to the VO4 groups. Black dashed circles depict partially occupied oxygen, light grey circles correspond to the fully occupied oxygen atoms and small grey circles represent Bi.

configurations, the $6s^2$ lone pair of Bi^{III} is always active (Fig. 3d). Further details of the Bi–O distances can be obtained from the supporting information available, see below.

3.2. Structure of $Bi_{46}P_8O_{49}$

A similar procedure as for the structure of $Bi_{46}V_8O_{49}$, was used to solve the structure. A standard peak search on the recorded frames followed by a refinement showed that the symmetry is monoclinic. A reciprocal space reconstruction were performed and revealed that in contrast to $Bi_{46}V_8O_{89}$ all the peaks can be indexed in a C centring-Bravais lattice (Fig. 4). Crystal data and experimental conditions of the data collection are gathered in Table 5. The structure was solved by the heavy-atom method. In a first stage, 14 Bi atoms have been localised corresponding to the total number of bismuth atoms in the structure. However, the refinement revealed that the isotropic displacement parameter of the Bi14 atom is high compared to the other bismuth atoms. A Fourier map around the Bi14 position shows clearly that this position is split in two positions Bi14 and Bi14*a* with an occupancy 1/3 and 2/3, respectively (Table 6). The independent phosphorous positions and the oxygen sites have been deduced from successive Fourier maps (Table 6). As for the structure of $Bi_{46}V_8O_{89}$ refined in the C centring Bravais lattice, the refinement revealed that the isotropic displacement of the oxygen atoms (O1 to O12) bonded to the phosphorous atoms are large compared to other oxygen sites (Table 6). Moreover a spilt position for the oxygen atoms surrounding the P2 atom have been introduced in the refinement (Table 6). The partially occupied oxygen positions have also been deduced from a difference Fourier map. They correspond to the four positions O29 to O32 (Table 6). The refinement converged to $R = 0.0566$ considering anisotropic displacement parameters for Bi and P and isotropic displacement parameters for the oxygen atoms. At this stage, a final difference Fourier map revealed significant and systematic residues ($\approx 6e^-/\AA^3$) around each Bi sites except the split Bi14 and Bi14*a* sites. For a better description of the electronic density around those sites, an expansion of the atomic displacement parameter was introduced [13]. Gram-Charlier expansions [14] to the third order for the Bi sites were used. Site-symmetry restrictions were applied on tensor components [15]. Although many non-harmonic coefficients were non-significant at the end of the refinement, they were not fixed to zero because there is a satisfactory ratio between the number of refined parameters (367) and the number of independent reflections (4058). The reliability factors dropped to

Table 4
Bond lengths (Å) and bond angles (deg) for the VO4 tetrahedra in $Bi_{46}V_8O_{89}$

V1–O35	1.56(4)	V1–O37	1.65(4)	V1–O39	1.63(4)
V1–O41	1.81(2)	V2–O36	1.70(2)	V2–O38	1.65(4)
V2–O40	1.66(4)	V2–O42	1.75(4)	V3–O27	1.66(4)
V3–O29	1.71(4)	V3–O31	1.68(2)	V4–O28	1.74(2)
V4–O30	1.72(2)	V4–O32	1.66(2)	V4–O34	1.72(4)
O35–V1–O37	114(2)	O35–V1–O39	110(2)	O35–V1–O41	113(2)
O37–V1–O39	106(2)	O37–V1–O41	108(2)	O39–V1–O41	105(2)
O36–V2–O38	112(2)	O36–V2–O40	114(2)	O36–V2–O42	107(2)
O38–V2–O40	107(2)	O38–V2–O42	110(2)	O40–V2–O42	108(2)
O27–V3–O29	107(2)	O27–V3–O31	111(2)	O27–V3–O33	111(2)
O29–V3–O31	112(1)	O29–V3–O33	107(1)	O31–V3–O33	107(1)
O28–V4–O30	107(1)	O28–V4–O32	110(1)	O28–V4–O34	109(1)
O30–V4–O32	114(1)	O30–V4–O34	110(1)	O32–V4–O34	107(1)

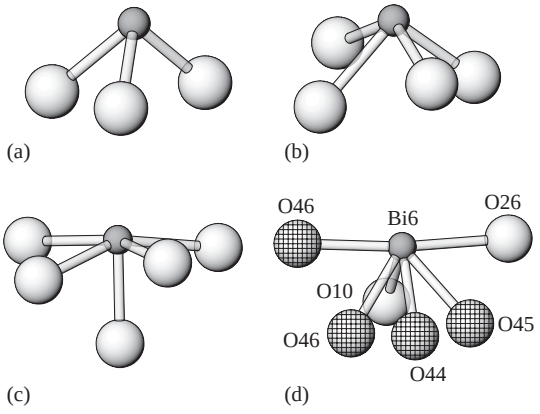

Fig. 3. Polyhedra around the Bismuth in $Bi_{46}V_8O_{89}$ (a) CN = 3, (b) CN = 4, (c) CN = 5 and (d) for the partially occupied oxygen sites (dashed circles, see text).

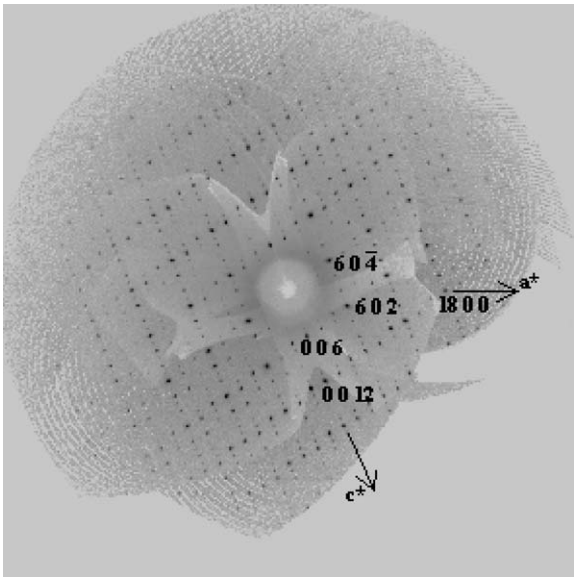

Fig. 4. (*h*0*l*) plane of $Bi_{46}P_8O_{89}$.

the R values $R = 0.0474$, $wR(F2) = 0.0881$ (g.o.f. = 1.20) (Table 5). No significant density was found in the vicinity of the Bi sites as it is shown, for example, in Fig. 5 for the Bi9 site.

A view of the $Bi_{46}P_8O_{89}$ structure is given in Fig. 6. As in the structure of $Bi_{46}V_8O_{89}$, the PO4 tetrahedra are perfectly well isolated ones from the others. The P–O distances are compiled in Table 7. The Bi atoms have environments similar to those observed in the structure of $Bi_{46}V_8O_{89}$ (Fig. 3). Further details on the structure can be obtained from the supporting material. One can notice that the Bi–O minimum distance of 2.01(3) Å is consistent with such environments found in Sillenite phases [16]. In $Bi_{46}P_8O_{89}$, four positions (O29–O32) are partially filled by oxygen that can participate to the pathway of the oxygen ionic conductivity. Each position has a multiplicity of height (8*j* position) and they are occupied by 18 oxygen atoms. Therefore, at least one position is more than half occupied. Several configurations can be imagined that fulfilled the global composition and are compatible with oxygen–oxygen distances. For example, if the O31 site is fully occupied, the ten oxygen missing can be located on O29 and or O32 sites but not on O30 site ($d_{O31-O30} = 0.77$ Å). The other O–O distances are longer than 2.42 Å.

As mentioned before, both structures correspond to a fluorite-type superstructure where the Bi and V atoms are perfectly ordered. The structures can be viewed as the stacking of two types of layers with the composition $[Bi_{18}O_{27}]$ and $[Bi_{14}M_4O_{31}]$ (M = P, V), respectively (Fig. 7). For clarity, the oxygen atoms have been omitted in Fig. 7. These layers are parallel to (001) of the monoclinic unit-cell which corresponds to (−1−11) of the fluorite sub cell. The periodicity of the structure is defined by the stacking of six layers with two times the sequence: 2 $[Bi_{14}M_4O_{31}]$layers + 1 $[Bi_{18}O_{27}]$ layer (Fig. 7). The change of space group from $C2/m$ for $Bi_{46}P_8O_{89}$ to $P2_1/c$ for $Bi_{46}V_8O_{89}$ results only of a

Table 5
Crystallographic data for $Bi_{46}P_8O_{89}$

Physical, crystallographic and analytical data	
Formula	$Bi_{46}P_8O_{89}$
Crystal colour	Pale green
MW ($g\,mol^{-1}$)	11284.8
Crystal system	Monoclinic
Space group	$C2/m$
Parameters	$a = 19.6073(3)$ Å, $b = 11.4181(2)$ Å, $c = 21.1119(3)$ Å, $\beta = 112.14(2)^\circ$
V (Å^3)	4378.0(6)
Z	2
Density calc. ($g\,cm^{-3}$)	8.558
Crystal shape	Unshaped
Crystal size (mm)	$0.076 \times 0.050 \times 0.016$
Data collection	
Temperature	RT
Diffractometer	Bruker-Nonius KappaCCD
Radiation	MoK_α ($\lambda = 0.71069$ Å)
Scan mode	CCD scan
hkl range	$-35<h<35$ $-20<k<20$ $-38<l<32$
θ_{max}	40°
Data reduction	
Linear absorption coeff.	$92.32\,mm^{-1}$
Absorption correction	Gaussian
T_{min}/T_{max}	0.016/0.234
No of reflections	14088
No of independent reflections	4058
Criterion for obs. reflections	$I > 3\sigma(I)$
Refinement results	
Refinement	F^2
$F(000)$	9300
R factors	$R(F) = 0.0474$ $wR(F^2) = 0.0881$
No of refined parameters	367
g.o.f.	1.20
Weighting scheme	$w = 1/(\sigma^2(I) + 0.0009I^2)$
Diff. Fourier residues (e$^-$/Å^3)	[−2.69, +2.72]

different repartition of the M atoms in the $[Bi_{14}M_4O_{31}]$ layer but the stacking of the layers is identical in both cases (Fig. 7). From this description, the composition and the structure of different phases can be predicted resulting from different stacking sequences of these two types of layers. The basic principle could be comparable to that of the well known hexagonal polytype perovskites. By this way, one could explain the large domain of 'solid-solution derived from fluorite' observed in the two systems [4–9]. The first member of this new family related to the fluorite-type structure correspond to the simplest sequence where all the layers have the composition $[Bi_{14}M_4O_{31}]$. Really, it has been shown [17] that the structure of the new phosphate $Bi_{14}P_4O_{31}$ corresponds to this member where all the layers have the predicted composition and where the PO4 tetrahedra are isolated ones from the others as proposed by the building principle. The proposed structural model can easily be extrapolated to other types of layers as, for example, the stacking of $[Bi_{18}O_{27}]$ layers and layers with composition $[Bi_{12}M_6O_{33}]$. The key of the building principle is when you replace one bismuth by one vanadium in 'Bi_2O_3' you add one oxygen atom to preserve the charge balance. Also, one postulate for symmetry conditions that the number of vanadium should be even in each layer.

4. Conclusions

The structures of $Bi_{46}P_8O_{89}$ and $Bi_{46}V_8O_{89}$ have been determined on single crystal. Both structures crystallise really in the monoclinic symmetry and have a fluorite-type superstructure with $3 \times 3 \times 3$ subcells. The M atoms (M = P, V) and the bismuth atoms are well ordered in the lattice but with different cationic order what explain the change of space group. The MO4 tetrahedra are well isolated ones from the others which contradicts the previous structural hypothesis. The

Table 6
Final coordinates, equivalent displacement parameters (Bi, P) and isotropic displacement parameters (O) for $Bi_{46}P_8O_{89}$

Atoms	Wyckoff Positions	Occupancy	x	y	z	$U_{eq}(Å^2)/U_{iso}(Å^2)$
Bi1	4*i*	1	0.0813(1)	$\frac{1}{2}$	0.7437(1)	0.028(1)
Bi2	8*j*	1	0.41013(9)	0.1679(1)	0.74153(9)	0.0174(3)
Bi3	8*j*	1	0.20282(9)	0.6677(2)	0.91851(8)	0.0216(3)
Bi4	8*j*	1	0.2586(1)	0.6644(2)	0.7674(1)	0.0302(4)
Bi5	4*i*	1	0.0384(1)	0	0.4234(1)	0.0230(4)
Bi6	4*i*	1	0.2556(1)	$\frac{1}{2}$	0.2441(1)	0.0258(5)
Bi7	8*j*	1	0.37209(8)	0.8383(2)	0.92520(8)	0.0177(3)
Bi8	8*j*	1	0.0792(1)	0.1759(2)	0.74381(9)	0.0327(4)
Bi9	4*i*	1	0.3067(2)	$\frac{1}{2}$	0.0887(1)	0.0357(6)
Bi10	8*j*	1	0.29621(8)	0.3378(2)	0.57892(8)	0.0204(3)
Bi11	8*j*	1	0.1348(1)	0.8416(2)	0.59521(9)	0.0267(4)
Bi12	8*j*	1	0.96575(9)	0.3275(1)	0.57391(8)	0.0173(3)
Bi13	8*j*	1	0.02918(9)	0.8359(2)	0.90650(8)	0.0186(3)
Bi14	4*i*	0.34	0.0730(3)	0	0.2384(2)	0.0256(7)
Bi14*a*	4*i*	0.66	0.0924(1)	0	0.2678(1)	0.0256
P1	4*i*	1	0.3737(5)	$\frac{1}{2}$	0.9274(5)	0.021(3)
P2	4*i*	1	0.1373(5)	$\frac{1}{2}$	0.6007(6)	0.024(3)
P3	4*i*	1	0.0308(4)	$\frac{1}{2}$	0.8951(4)	0.015(2)
P4	4*i*	1	0.2971(4)	0	0.5888(4)	0.018(3)
O1	4*i*	1	0.427(3)	$\frac{1}{2}$	0.887(2)	0.11(1)
O2	8*j*	1	0.389(2)	0.606(3)	0.973(1)	0.100(8)
O3	4*i*	1	0.295(2)	$\frac{1}{2}$	0.878(2)	0.068(8)
O4	8*j*	0.5	0.010(2)	0.386(4)	0.558(2)	0.068(8)
O4*a*	4*i*	0.5	0.087(3)	$\frac{1}{2}$	0.528(3)	0.068
O5	4*i*	0.5	0.149(3)	$\frac{1}{2}$	0.676(3)	0.068(8)
O5*a*	8*j*	0.5	0.123(2)	0.123(2)	0.647(2)	0.068
O6	4*i*	1	0.219(2)	$\frac{1}{2}$	0.610(2)	0.09(1)
O7	4*i*	1	0.953(2)	$\frac{1}{2}$	0.893(2)	0.09(1)
O8	4*i*	1	0.023(2)	$\frac{1}{2}$	0.819(2)	0.082(9)
O9	8*j*	1	0.073(1)	0.606(3)	0.930(1)	0.086(7)
O10	8*j*	1	0.344(1)	0.113(2)	0.600(1)	0.072(6)
O11	4*i*	1	0.256(2)	0	0.633(2)	0.069(8)
O12	4*i*	1	0.236(1)	0	0.515(1)	0.058(7)
O13	8*j*	1	0.8915(6)	0.180(1)	0.5515(6)	0.020(2)
O14	8*j*	1	0.1316(6)	0.189(1)	0.8914(6)	0.022(2)
O15	4*i*	1	0.355(1)	$\frac{1}{2}$	0.616(1)	0.033(4)
O16	4*i*	1	0.4990(9)	$\frac{1}{2}$	0.7076(8)	0.021(4)
O17	8*j*	1	0.0449(7)	0.816(1)	0.6282(7)	0.030(3)
O18	4*i*	1	0.315(1)	0	0.8971(9)	0.029(4)
O19	4*i*	1	0.1671(9)	0	0.8061(9)	0.024(4)
O20	4*i*	1	0.0779(8)	0	0.5393(8)	0.018(3)
O21	8*j*	1	0.4779(7)	0.689(1)	0.7989(7)	0.030(3)
O22	8*j*	1	0.1966(8)	0.188(2)	0.7169(8)	0.041(4)
O23	8*j*	1	0.3473(8)	0.691(1)	0.6865(7)	0.036(3)
O24	4*i*	1	0.056(1)	0	0.876(1)	0.040(5)
O25	4*i*	1	0.142(1)	0	0.666(1)	0.052(6)
O26	8*j*	1	0.996(1)	0.670(2)	0.700(1)	0.060(5)
O27	8*j*	0.5	0.021(1)	0.757(2)	0.514(1)	0.028(6)
O28	8*j*	1	0.156(1)	0.355(2)	0.795(1)	0.065(5)
O29	8*j*	0.75	0.282(1)	0.803(2)	0.956(1)	0.047(3)
O30	8*j*	0.5	0.321(2)	0.205(3)	0.824(2)	0.047
O31	8*j*	0.5	0.355(2)	0.210(3)	0.814(2)	0.047
O32	8*j*	0.5	0.262(2)	0.238(3)	0.862(2)	0.047

partially occupied oxygen sites have been determined which can explain the pathway of the ionic oxygen conductivity of these phases. A structural building principle has been proposed that can explain the large domain of solid solution related to the fluorite-type, observed in the two systems. A complete re-investigation of the two systems is in progress in order to isolate new members of this series.

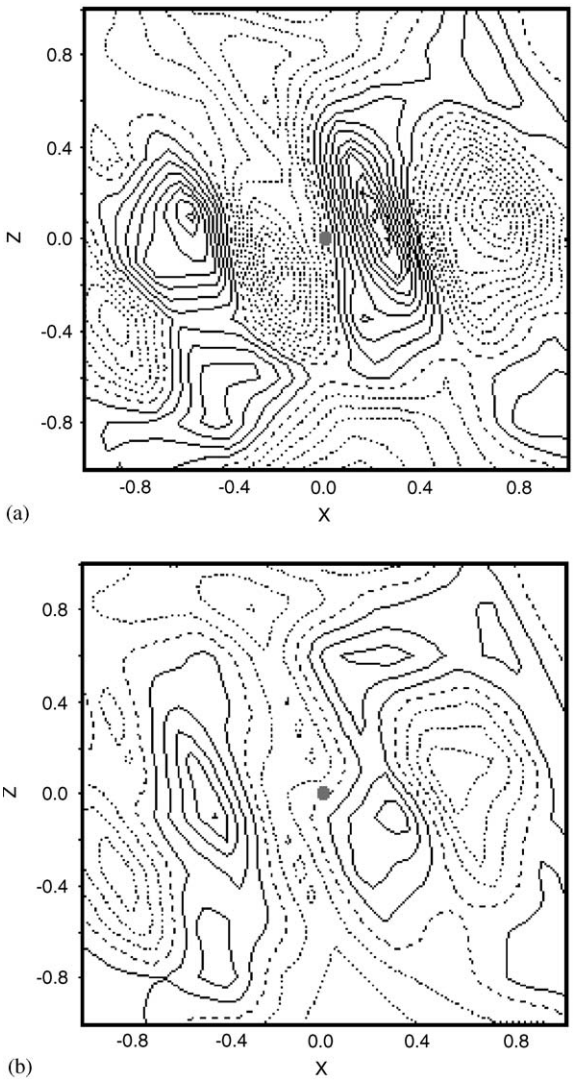

Fig. 5. Difference Fourier maps around the Bi9 position for $Bi_{46}P_8O_{89}$. (a) harmonic refinement; (b) non-harmonic refinement. Both *xz* sections at $y = 0.5$. Bi9 indicates by (●). Negative contour lines (dashed lines), positive contour lines (continuous lines), contour lines in intervals of $0.5\,e/Å^3$.

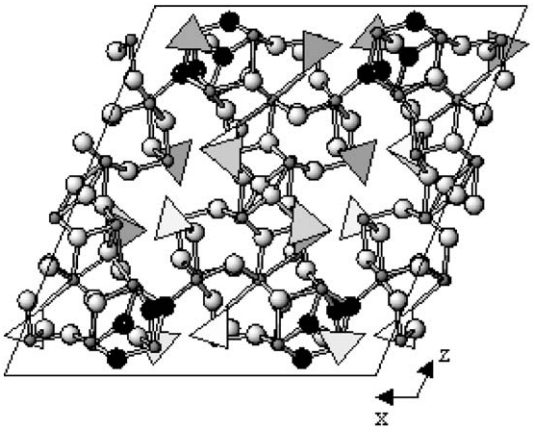

Fig. 6. View of the $Bi_{46}P_8O_{89}$ structure projected on the (010) plane. Tetrahedra correspond to the PO4 groups. Black dashed circles depict partially occupied oxygen, light grey circles correspond to the fully occupied oxygen atoms and small grey circles represent Bi.

Table 7
Bond lengths (Å) and bond angles (deg) for the PO4 tetrahedra in $Bi_{46}P_8O_{89}$

P1–O1	1.58(6)	2xP1–O2	1.51(3)	P1–O3	1.50(3)
P2–O5	1.52(7)	2xP2–O4	1.59(4)	P2–O6	1.54(4)
P2–O4*a*	1.48(5)	2xP2–O5*a*	1.62(5)	P3–O7	1.51(4)
P3–O8	1.59(4)	2xP3–O9	1.49(3)	P4–O11	1.44(5)
P4–O12	1.57(2)	2xP4–O10	1.55(2)		
O1–P1–O2	110(2)	O1–P1–O3	110(2)	O2–P1–O2	107(2)
O2–P1–O3	110(2)	O4–P2–O4	109(2)	O4–P2–O5	117(2)
O4–P2–O6	108(2)	O5–P2–O6	97(3)	O7–P3–O8	107(2)
O7–P3–O9	112(1)	O8–P3–O9	108(1)	O9–P3–O9	108(1)
O10–P4–O10	113(1)	O10–P4–O11	110(1)	O10–P4–O12	109.8(9)
O11–P4–O12	104(1)				

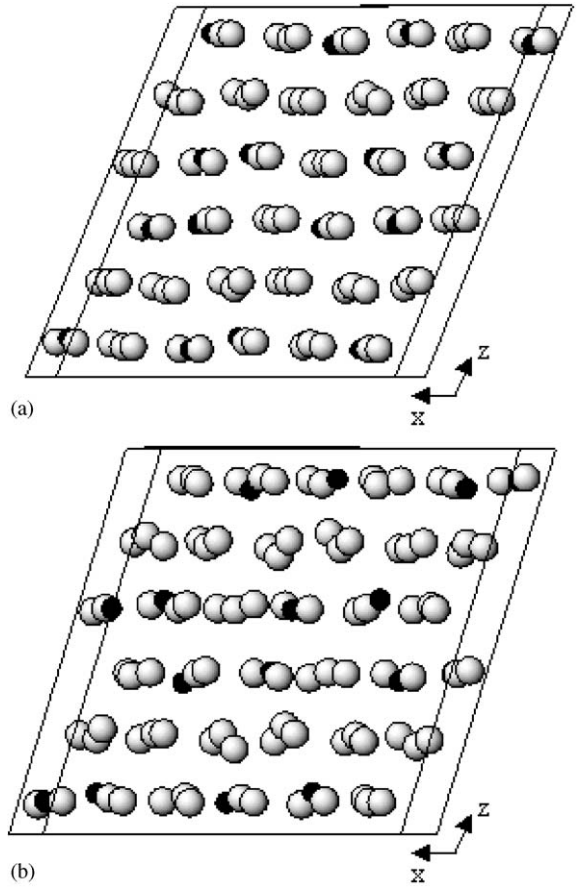

Fig. 7. View of the $[Bi_{18}O_{27}]$ and $[Bi_{14}M_4O_{31}]$ layers (M = P, V) parallel to the (001) plane. (a) for $Bi_{46}P_8O_{89}$; (b) $Bi_{46}VO_{89}$. Filled circles (M atoms); light grey circles (Bi). The oxygen atoms have been omitted.

4.1. Supporting information available

Further details of the crystal structure investigation can be obtained from the supporting information available from the Fachinformationszntrum Karlsruhe,

76344 Eggenstein-Leopoldshafen, Germany, (fax: (49) 7247-808-666; email: mailto:crysdata@fiz-karlsruhe.de) on quoting the depository number CSD-415113 ($Bi_{46}V_8O_{89}$) and CSD-415114 ($Bi_{46}P_8O_{89}$).

References

[1] G. Gattow, H.Z. Schröder, Z. Anorg. Allg. Chem. 318 (1962) 176.
[2] H.A. Harwig, Z. Anorg. Allg. Chem. 444 (1978) 151.
[3] T. Takahashi, H. Iwahara, Mater. Res. Bull. 13 (1978) 1447.
[4] W. Zhou, J. Solid State Chem. 76 (1988) 290.
[5] W. Zhou, J. Solid State Chem. 87 (1990) 44.
[6] S. Kashida, T. Hori, K. Nakamura, J. Phys. Soc. Japan 63 (1994) 4422.
[7] S. Kashida, T. Hori, J. Solid State Chem. 122 (1996) 358.
[8] A. Watanabe, Solid State Ionics 96 (1997) 75.
[9] A. Watanabe, Y. Kitami, Solid State Ionics 113–115 (1998) 601.
[10] A.J.M. Duisenberg, L.M.J. Kroon-Batenburg, A.M.M. Schreurs, J. Appl. Cryst. 36 (2003) 220.
[11] V. Petricek, M. Dusek, The Crystallographic Computing System Jana 2000, Institute of Physics, Praha, Czech Republic.
[12] R. Enjalbert, J. Galy, Acta Crystallogr. 1467–1469 (1986) C42.
[13] R. Bachmann, H. Schulz, Acta Crystallogr. A 668–675 (1984) 40.
[14] C.K. Johnson, H.A. Levy, International Tables for X-ray Crystallography, Vol. IV, Kynoch Press, Birmingham, pp. 311–336. (Present distributor Kluwer Academic Publishers, Dordrecht.)
[15] W.F. Kuhs, Acta Crystallogr. A 133–137 (1984) 40.
[16] J.L. Soubeyroux, M. Devalette, N. Khachani, P. Hagenmuller, J. Solid State Chem. 59–63 (1990) 86.
[17] F. Mauvy, J.C. Launay, J. Darriet, J. Solid State Chem., submitted for publication.